DE89-004302

SHIELD OPTIMIZATION PROGRAM, PART II: EFFECTS OF VAN ALLEN BELT RADIATION ON SDI WEAPON PLATFORMS

Oak Ridge National Laboratory
Oak Ridge, TN

19980513 127

Dec 88

U.S. DEPARTMENT OF COMMERCE
National Technical Information Service
NTIS

U01809

Accession Number: 1809

Publication Date: Dec 01, 1988

Title: Shield Optimization Program, Part II: Effects of Van Allen Belt Radiation on SDI Weapon Platforms

Personal Author: Barnes, J.M.; Santoro, R.T.; Johnson, J.O., et al.

Corporate Author Or Publisher: Oak Ridge National Laboratory, Oak Ridge, TN 37831 Report Number: ORNL/TM-10957

Report Prepared for: U.S. Dept. of Energy

Descriptors, Keywords: Van Allen Radiation Weapon Platform Space SDI Shielding Rad/Hard Damage Interceptor SBI Detection Proton Electron KKV Material Model

Pages: 045

Cataloged Date: May 30, 1989

Contract Number: DE-AC05-84OR21400

Document Type: HC

Number of Copies In Library: 000001

Original Source Number: DE89-004302

Record ID: 20692

Source of Document: NTIS

NOT IN PROCS

DE89004302

ORNL/TM-10957

OAK RIDGE
NATIONAL
LABORATORY

MARTIN MARIETTA

Shield Optimization Program, Part II: Effects of Van Allen Belt Radiation on SDI Weapon Platforms

J. M. Barnes
R. T. Santoro
J. O. Johnson
J. D. Drischler
T. A. Gabriel
M. S. Smith

OPERATED BY
MARTIN MARIETTA ENERGY SYSTEMS, INC.
FOR THE UNITED STATES
DEPARTMENT OF ENERGY

Printed in the United States of America. Available from
National Technical Information Service
U.S. Department of Commerce
5285 Port Royal Road, Springfield, Virginia 22161
NTIS price codes—Printed Copy: A04; Microfiche A01

ORNL/TM-10957

Engineering Physics and Mathematics Division

Shield Optimization Program, Part II: Effects of Van Allen Belt Radiation on SDI Weapon Platforms

J. M. Barnes,* R. T. Santoro, J. O. Johnson,
J. D. Drischler, T. A. Gabriel, M. S. Smith

DATE PUBLISHED — December 1988

*Computing and Telecommunications Division

Prepared by the
OAK RIDGE NATIONAL LABORATORY
Oak Ridge, Tennessee 37831
operated by
MARTIN MARIETTA ENERGY SYSTEMS, INC.
for the
U.S. DEPARTMENT OF ENERGY
under contract DE-AC05-84OR21400

CONTENTS

LIST OF FIGURES

LIST OF TABLES

ABSTRACT

The effects of both natural and man-made Van Allen Belt (VAB) radiation at an altitude of 500 km are presented for various components of a prototypic space-based interceptor (SBI) weapon platform. The weapon platform is described in detail and represents the authors' concept of such a system. The calculated results show that the SBI platform will survive long term (10 years) exposure to natural VAB protons and electrons. However, when the electron belts are enhanced by the detonation of a nuclear weapon, high levels of radiation can be expected in components mounted on or near the surface of the spacecraft. These dose levels are sufficient enough to produce damage in the most sensitive components.

 Preceding page blank

1. INTRODUCTION

The Strategic Defense Initiative Organization (SDIO) has proposed the deployment of a space-based weapon system as a deterrent to attack on the United States by intercontinental ballistic missiles (ICBM). This defensive system will consist of tiers of sensor satellites and weapon platforms at different altitudes to detect, track, and destroy rising ICBMs. The lowest tier will consist of space-based interceptor (SBI) weapon platforms in low earth orbits. The middle tier will consist of Space Surveillance and Tracking Systems (SSTS) platforms in mid-earth orbits. The upper tier will consist of Boost-Phase Surveillance and Tracking Systems (BSTS) platforms in geosynchronous orbits. To ensure that these platforms carry out their missions, they must have the capability to survive long-term (up to 10 years) exposure to the natural radiation in space and the transient effects of man-made radiation introduced by nuclear weapon detonations or directed particle beams. In addition, the on-board shielding must also ensure survivability against space debris and kinetic energy weapon projectiles, and harassment and interdiction by ground and space-based laser weapons.

The Optimization Program was initiated to optimize nuclear performance of shields. SBI and SSTS are studied since they have need for advanced kinetic energy weapon (KEW) and laser shielding. Studies of the nuclear environment and its effects on SDI platforms and shielding are required so that the benefits of added shielding can be determined and application methods, materials, and shield designs can be identified which optimize the shields survivability and the shields nuclear mitigation capability. In the future, the SSTS platform and more realistic SBI orbital inclinations will be studied with various levels of added KEW shielding and applied optimization techniques.

This paper presents the results of Monte Carlo radiation transport calculations to estimate the effects of natural (proton and electron) and nuclear enhanced (pumped) electron Van Allen Belt (VAB) radiation on the components of a prototypic SBI platform. The SBI platform and the kinetic kill vehicle (KKV) weapons are described in Section 2. The VAB spectra, Monte Carlo codes, and calculational methods used to estimate the radiation damage to the platform and its components are described in Section 3. The results are presented and discussed in Section 4.

It should be noted that the SBI platform used in this study represents the authors' concept of such a system and it is not that proposed for deployment by the SDIO. The platform design is based, in part, on space weapon system requirements eluded to in the Defense Acquisition Board documents on SDI space weapon-sensor architecture requirements and also from information gained at briefings given by other groups involved in weapon platform design. In "designing" the ORNL platform, every effort has been made to protect proprietary information or contractor configurations.

2. CALCULATIONAL MODEL OF THE WEAPON PLATFORM

2.1 DESCRIPTION

The Oak Ridge National Laboratory (ORNL) weapon platform, shown in Figure 1a, is a cylindrical shell comprised of two interceptor-fuel tank (IFT) modules connected by a command, control, and communications (C^3) bay. Each IFT module contains five launch tube-kinetic kill vehicle (KKV) assemblies and four fuel tanks. The platform has an overall length of 4.27 m and a diameter of 1.63 m. Figure 1b is an exploded view showing the interior of the platform and the orientation of the KKV launch tubes and fuel tanks. Fuel storage is required for maneuvering the platform to avoid collisions with space debris, evading enemy kill vehicles and KEW projectiles, and positioning the platform during engagement.

Power is supplied to on-board electronic and electrical circuits by two solar panels, one on each side of the platform. These are shown in Figure 1a in the deployed position. During conflict, the panels may be folded along the top of the platform to reduce the cross-sectional area of the SBI that is exposed to attack by enemy weapons. A shield to protect the SBI against ground based laser attack covers the surfaces of the IFT and C^3 bays that are exposed to the earth. A single antenna, mounted on the top of the platform, provides communication with the sensor and battle management satellites in the upper tiers of the defense network.

Figure 1c shows the C^3 bay. The electronic systems are housed in two concentric, thin walled ring shaped containers. In the center is a box for housing "critical" or sensitive components. The rationale for designing the C^3 bay in this manner allows components that are insensitive to radiation to be mounted in the outer ring while more radiation sensitive components may be placed in the inner ring or the central box. Allowance has been made for the addition of local shielding to be placed in the spaces between the outer and inner rings for increasing the radiation protection of critical or sensitive components.

A prototypic kinetic kill vehicle is shown in Figure 2a. The main components of the weapon are the warhead, sensors for guiding the interceptor to the target, fuel, and the rocket motor. Figure 2b shows the KKVs mounted in the launch tubes of the IFT.

Other systems that may be essential in an SBI platform, i.e., thermal control equipment, etc., were not included in the calculational model. The principal concern here was to represent subsystems that are

a. most sensitive to radiation damage and
b. essential to the wartime mission.

2.2 DETAILS OF THE SBI PLATFORM AND INTERCEPTORS

The SBI platform shell, contents, solar panels, and KKV interceptors were modeled using the Combinatorial Geometry (CG) package that is available for use with the Monte Carlo radiation transport codes HETC (1), MORSE (2),

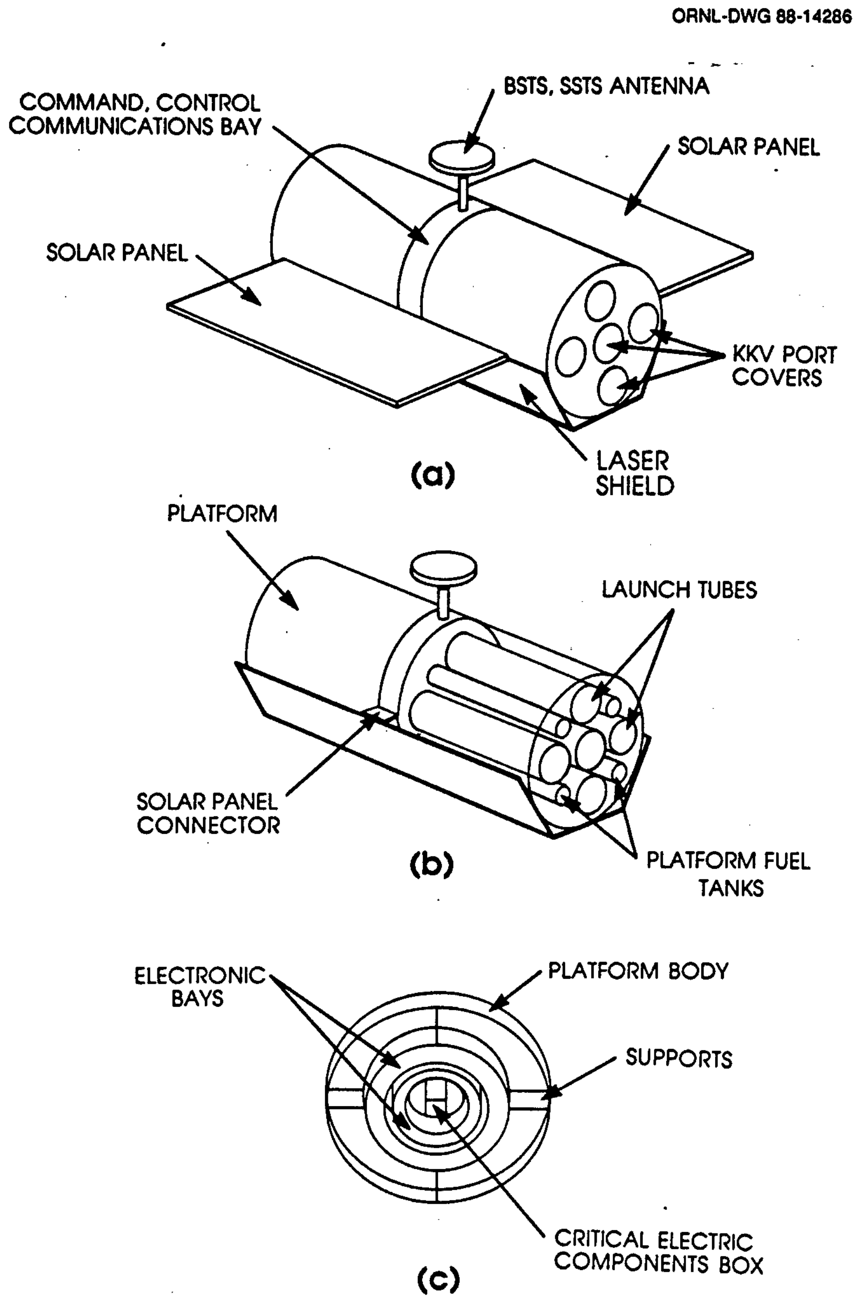

Figure 1. Calculational Model of the Space Based Interceptor Weapon Platform (a), with Interior views showing Launch Tube-Fuel Tanks Cluster (b), and the Central C^3 Bay (c).

ORNL-DWG 88-14287

(a)

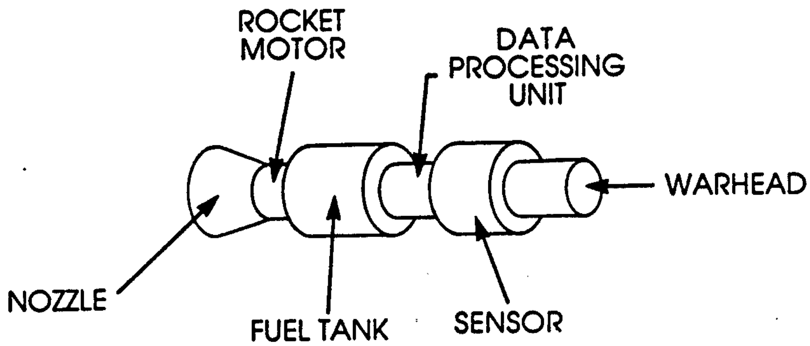

(b)

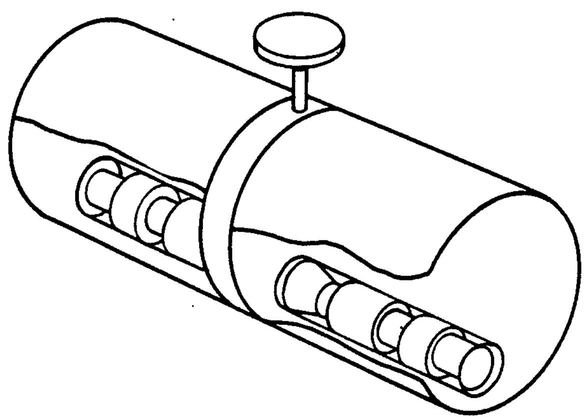

Figure 2. Kinetic Kill Vehicle (a) and Exploded View of SBI Weapon Platform Showing KKVs Inside Launch Tubes (b).

MICAP (3), and EGS (4). Figures 1(a,b,c) and 2(a,b) were, in fact, generated with the JUNEBUG (5) plotting code using the CG logic and descriptors as input. The advantage of using CG to model the platform is that the geometry is interchangeable in the various Monte Carlo codes thereby ensuring consistent analyses.

The SBI platform structure, structural support members, KKV launch tubes, C^3 bay, and fuel tanks were "constructed" with 0.32 cm-thick aluminum. One interceptor launch tube is on the central axis of the IFT module and the remaining four are placed at 90 degrees to each other on a 0.51 m radius from the centerline of the IFT to the axis of the tube. The 1.98 m-long KKV launch tubes have an inner radius of 0.21 m. The 1.97 m-long by 0.2032 m diameter fuel tanks are on the same radius and located alternately with the launch tubes. The fuel was taken to be hydrazine having a density of 1 g/cm^3. The quantity of fuel was arbitrarily chosen to maintain the overall weight of the platform (~3000 kg). The launch tubes and fuel tanks are connected to the IFT assembly and to each other by 0.32 cm-thick aluminum structural supports.

The central C^3 bay has an axial dimension of 0.31 m. The radial thickness of the outer shell is 0.15 m (inner radius = 0.55 m) and the inner shell has a radial thickness of 0.10 m (inner radius = 0.21 m). The central box has cross-sectional dimensions of 0.15 m by 0.15 m and has an overall axial dimension of 0.298 m.

The solar panels are 3.41 m-long, 1.71 m-wide and 0.05 m-thick and have an active area of 11.7 m^2. The KKVs are 1.97 m-long and have a maximum radius of 0.20 m.

The laser shield is a thin (0.01 m-thick) carbon layer. It is recognized that this shield is too thin to provide adequate protection against intense laser attack. It is included only for providing first order estimates of its radiation shielding effectiveness. Kinetic energy weapon shielding has been omitted since there is currently some uncertainty in the location of these shields, i.e., directional versus full coverage.

Complete geometric descriptions of the components of the SBI platform and the KKVs are given in Table 1. The column labeled "CG Body Type" defines the shape of each component. Two-hundred forty-three body descriptors were required to describe the platform. A complete listing of the CG input for use in the various codes is given in Appendix A. Tables 2 and 3 list the material compositions of the platform components and KKVs, respectively. In some cases, e.g., the electronic and electrical systems, the components are very idealized and the material densities have been reduced to account for the distributions of sub-components. Also included in these tables are the volumes and weights of each element. The weight of the empty SBI platform including the solar panels is 2030.15 kg. Each KKV weighs 69.16 kg, so when deployed and fully loaded, the total weight of the platform is 2722 kg.

Table 1

Components and Dimensions of the SBI Weapon Platform

Component	CG Body Type	Volume (cm^3)	Dimensions (cm)
Solar Panel	BOX	291,350.76	l=341.38,w=170.69,h=5.0
Solar Panel Connector	BOX	1,524.00	l=30.48,w=20.0,h=5.0
Antenna Support	RCC	3,926.99	r=5.0, h=50.0
Antenna	RCC	38,484.51	r=35.0, h=10.0
Laser Shield	BOX	111,629.95	l=426.42,w=101.6,h=1.0 (base) l=426.42,w=80.0,h=1.0 (sides)
Platform (2 parts)	RCC	39,082.64	r=81.6, h=198.12
Instrument Bay Housing	RCC	18,273.98	r=81.6, h=30.48
Instrument Bay Box	BOX	6,021.32	l=29.20,w=14.36,h=14.36
Instrument Bay Box Walls	BOX	692.68	l=29.84,w=15.0,h=15.0
Most Inner Circular Instr. Bay Wall	RCC	1,509.52	r=25.32, h=29.84
Inner Circular Instrument Bay	RCC	52,647.26	r=35.0, h=29.84
Inner Circular Instrument Bay Wall	RCC	2,090.30	r=40.0, h=29.84
Outer Circular Instrument Bay Wall	RCC	2,409.47	r=40.32, h=29.84
Outer Circular Instrument Bay	RCC	127,887.10	r=54.68, h=29.84
Outer Circular Instrument Bay Wall	RCC	3,290.23	r=55.0, h=29.84
Instrument Bay Support Beam (4)	BOX	201.83	l=24.0,w=0.32,h=26.28
KKV Tube (10)	RCC	8,158.08	r=20.64, h=198.12(outer) r=30.32, h=198.12(inner)
Fuel Tank (8)	RCC	8,573.18	r=10.48, h=198.12
Fuel	RCC	256,580.45	r=10.16, h=197.8
Platform Support Beam (16)	BOX	1,225.41	l=197.8,w=0.32,h=60.74
KKV Tube Caps (10)	RCC	428.27	r=20.64, h=0.32
	KKV Components		
Nozzle	TRC	2,148.04	r1=19.68,r2=13.68,h=30.48
Motor Housing	RCC	635.73	r=14.0, h=15.24
Motor	RCC	8,748.33	r=13.68, h=14.92
Fuel Tank	RCC	2,602.52	r=20.0, h=45.72
Fuel	RCC	54,850.93	r=19.68, h=45.08
Computer Housing	RCC	1,224.44	r=14.0, h=30.48
Computer	RCC	9,423.26	r=10.68, h=29.84
Sensor Housing	RCC	1,994.59	r=20.00, h=30.48
Sensor	RCC	20,023.96	r=15.68, h=29.84
Head	RCC	18,768.13	r= 4.66, h=18.64

Table 2

Material Compositions for the SBI Weapon Platform

Component	Vol. (cm^3)	Material	Wt. (kg)
Solar Panel	291,350.76	Be-Si	552.11[a]
Solar Panel Connector	1,524.00	Al	4.11
Antenna Support	3,926.99	Al	10.60
Antenna	38,484.51	Si	17.70[b]
Laser Shield	111,929.95	C	223.86
Platform (2 parts)	39,484.51	Al	106.61
	39,484.51	Al	106.61
Instrument Bay Housing	18,273.98	Al	49.34
Instrument Bay Box	6,021.32	Si	2.77[b]
Instrument Bay Walls	692.68	Al	1.87
Most Inner Circle Instrument Bay Wall	1,509.52	Al	4.08
Circular Instrument Bay (Inner)	52,647.26	Si	24.22[b]
Circular Instrument Bay Wall (Inner)	2,090.30	Al	5.64
Circular Instrument Bay Wall (Outer)	2,409.47	Al	6.51
Circular Instrument Bay (Outer)	127,887.01	Si	58.83[b]
Circular Instrument Bay Wall (Outer)	3,290.23	Al	8.88
Circular Instrument Bay Support (4 Posts)	201.83	Al	2.18
KKV Tube (10)	8,158.08	Al	220.27
Fuel Tank (8)	2,143.30	Al	46.30
Fuel	64,145.11	N_2H_4	513.16
Platform Support Beams (16)	1,225.41	Al	52.94
KKV Tube Caps (10)	428.27	Al	11.56
		Total Weight	2030.15

[a]90% Beryllium – 10% Silicon (at 50% Density)
[b]Silicon at 20% Density

Table 3

Material Compositions for the Kinetic Kill Vehicles (Per KKV)

Component	Vol. (cm^3)	Material	Wt. (kg)	
Nozzle	2,148.04	CC	4.30	
Motor Housing	635.73	Al	1.72	
KKV Motor	8,748.33	SS	10.24	(15%)
Fuel Tank	2,602.52	Al	7.03	
Fuel	54,850.93	N_2H_4	13.71	(25%)
Computer Housing	1,224.44	Al	3.31	
Computer	9,423.26	Si	4.33	(20%) See Note A
Sensor Housing	1,994.59	Al	5.39	
Sensor	20,023.96	Si	9.21	(20%)
KKV Warhead	1,271.65	SS	9.92	
Total Weight			69.16	

KKV Warhead L/D = 2.0 = (18.64/9.32)
KKV Motor at 15% Density to Account for Structure.

Note A: Must ultimately insert a box inside this volume for housing a "computer."

3. VAN ALLEN BELT SPECTRA AND METHODS OF CALCULATION

The analysis of radiation induced effects in the platform were carried out assuming deployment of the SBI platform in a circular orbit at an altitude of 500 km and inclination angle of 0°. As the SBI orbits the earth, it passes through the Van Allen belts where it encounters proton and electron radiation at various flux levels. To determine the average particle flux, $\phi(E)$, incident on the spacecraft requires integration over time, i.e.,

$$\phi(E) = (1/T) \int_T \phi' \ (E, B(t)L(t)) \ dt \tag{1}$$

where $B(t)$ is the magnetic field intensity, $L(t)$ is the magnetic shell parameter, and T is a time that must be sufficiently large so that $\phi(E)$ is independent of T. The parameters B and L represent the components of a coordinate system that was developed by McIliwain (6) for mapping magnetically trapped particles. Several computer codes exist for calculating the time averaged particle spectra (7).

The angular distributions of the radiation incident on the SBI were assumed to be isotropic. This is necessary because of the lack of adequate proton and electron angular distribution data and because any other treatment could lead to poor results.

The differential VAB proton flux spectrum at 500 km is given in Table 4. The proton flux is not zero at energies below 30 MeV. However, since the outer skin of the SBI platform will stop most of the protons with energies below 30 MeV and since they would not contribute significantly to the total dose, the low energy portion of the analysis is cut off at 30 MeV to reduce code running time. The assumption is also made that the proton flux above 1000 MeV is zero since there are very few, if any, trapped protons at these high energies.

The differential natural VAB electron flux spectrum at 500 km is given in Table 5. In contrast to the proton spectrum, the electron energies are much lower, on the order of a few MeV. Since the range of these energy electrons in aluminum is small, they will not contribute to the damage to components that are protected by the platform skin. The majority of the damage to these components, particularly the electronics, arises from bremsstrahlung gamma rays produced by electron interactions.

The enhanced, or pumped, electron fluence spectrum arising from the detonation of a nuclear weapon (Starfish type) in space is given in Table 6. The total electron fluence as a function of time after the weapon is detonated is given in Table 7. These data were obtained by interpolating among calculated data for enhanced electron fluence spectra at altitudes of 403, 805, and 1610 km and at orbital inclination angles of 0, 30, 60, and 90 degrees. (8)

Note that the enhanced electron spectrum extends to higher energies than the natural electron spectrum and that the enhanced spectrum is also much harder. Also, it does not decay as rapidly after the burst. Because they have higher energies,

Table 4

The Differential Proton Flux Spectrum in the Van Allen Belt for a Circular Orbit at an Altitude of 500 Kilometers

Energy (MeV)	Differential Flux (protons/cm^2 · MeV · day)	Energy (MeV)	Differential Flux (protons/cm^2 · MeV · day)
30	4.400+04[a]	500	8.360+01
40	3.983+04	520	6.475+01
50	3.520+04	540	5.034+01
60	2.843+04	560	3.929+01
70	2.316+04	580	3.078+01
80	1.904+04	600	2.420+01
90	1.578+04	620	1.901+01
100	1.320+04	640	1.503−01
120	9.429+03	660	1.195−01
140	7.025+03	680	9.563+00
160	5.642+03	700	7.700+00
180	4.649+03	720	6.364+00
200	3.740+03	740	5.240+00
220	2.746+03	760	4.298+00
240	2.036+03	780	3.513+00
260	1.525+03	800	2.860+00
280	1.153+03	820	2.279+00
300	8.800+02	840	1.825+00
320	6.887+02	860	1.470+00
340	5.401+02	880	1.190+00
360	4.246+02	900	9.680−01
380	3.344+02	920	7.919−01
400	2.640+02	940	6.513−01
420	2.113+02	960	5.385−01
440	1.685+02	980	4.476−01
460	1.339+02	1000	3.740−01
480	1.060+02		

[a]Read as 4.400×10^4.

Table 5

The Differential Electron Flux Spectrum in the Van Allen Belt for a Circular Orbit at an Altitude of 500 Kilometers

Energy (MeV)	Differential Flux (electrons/cm^2 · MeV · day)	Energy (MeV)	Differential Flux (electrons/cm^2 · MeV · day)
0.05	4.320+10[a]	2.60	1.642+07
0.10	2.592+10	2.80	1.296+07
0.20	1.152+10	3.00	1.008+07
0.30	5.184+09	3.20	5.760+06
0.40	2.448+09	3.40	3.456+06
0.50	1.296+09	3.60	1.872+06
0.60	8.064+08	3.80	9.792+05
0.70	5.760+08	4.00	5.184+05
0.80	4.608+08	4.20	2.880+05
0.90	3.456+08	4.40	1.642+05
1.00	2.448+08	4.60	9.504+04
1.20	1.642+08	4.80	5.184+04
1.40	1.123+08	5.00	2.880+04
1.60	7.776+07	6.00	1.584+03
1.80	5.760+07	7.00	9.504+01
2.00	4.032+07	8.00	5.184+00
2.20	2.880+07	9.00	2.880−01
2.40	2.102+07	10.00	1.526−01

[a]Read as 4.320×10^{10}.

Table 6

The Normalized Differential Electron Fluence Spectrum Due to a High–Altitude Nuclear Burst for a Circular Orbit at an Altitude of 500 Kilometers

Lower Energy (MeV)	Differential Fluence (electrons/cm^2)
0.04	6.66–03[a]
0.25	5.40–02
0.50	1.28–01
1.00	3.45–01
2.00	2.66–01
3.00	1.28–01
4.00	4.73–02
5.00	1.78–02
6.00	6.19–03
7.00	1.65–03
10.00	—

[a]Read as 6.66×10^{-3}.

Table 7

Electron Fluence from a High–Altitude Nuclear Burst Versus Time after Detonation for a Circular Orbit at an Altitude of 500 Kilometers

Time After Detonation (days)	Electron Fluence (electrons/cm^2)
0.25	7.800+11[a]
1.00	2.420+12
2.00	4.580+12
7.00	1.268+13
30.00	3.100+13
60.00	4.880+13
180.00	9.560+13
365.00	1.422+14

[a]Read as 7.800×10^{11}.

these electrons have greater penetrating capability and may damage electronic components located inside the platform. To determine the total damage sustained from the combined effects of natural and enhanced VAB radiation requires summing the dose accumulated during orbits through the natural radiation environment with the dose received as a function of time after enhancement.

The radiation transport calculations to estimate the effects of VAB proton radiation were carried out using the Monte Carlo code HETC (1). The calculations to estimate the effects of natural electrons and enhanced electrons were performed using the Monte Carlo code EGS4. Complete descriptions of these codes are given in References 1, 4, and 9.

3.1 ENERGY AND ANGULAR BIASING OF THE INCIDENT SPECTRA

The radiation damage was calculated using energy and angular biasing of the incident source distributions. The unbiased source distributions for Van Allen belt natural proton and electron spectra and the nuclear enhanced electron spectra may be expressed in the form

$$J(E,\bar{\Omega}) = \Phi_o G(E,\vec{\Omega}), \tag{2}$$

where

$J(E,\vec{\Omega}) =$ the incident source particle current,
$\Phi_o =$ a normalization constant, and
$G(E,\bar{\Omega}) = F(E,\mu,\phi) =$ the unbiased probability density function (pdf) for source particles having energy E and directions $\mu = \cos\theta$ and ϕ.

The unbiased pdf is normalized so that

$$\int_{E_{\min}}^{E_{\max}} \int_o^1 \int_o^{2\pi} dE\, d\mu\, d\phi\, F(E,\mu,\phi) = 1 \tag{3}$$

for all particles having energies greater than the cutoff energy $E_{\min}$.

If $\Phi(E)$ is the omnidirectional (over 4π) flux spectrum, then

$$J(E,\bar{\Omega}) = \Phi(E)\left(\frac{\mu}{2}\right)\left(\frac{1}{2\pi}\right). \tag{4}$$

Integrating Eq. (4) over all directions and over all particle energies above the cutoff energy $E_{\min}$ leads to the normalization constant Φ_o; that is,

$$\Phi_o = \int_{E_{\min}}^{E_{\max}} dE\Phi(E) \int_o^1 d\mu\,\frac{\mu}{2} \int_o^{2\pi} d\phi\,\frac{1}{2\pi} = \frac{\psi(E_{\min}) - \psi(E_{\max})}{4}, \tag{5}$$

where

$$\psi(E) = \int_E^\infty \Phi(E')dE' .$$

Introducing $F(E,\mu,\phi) = f(E)\,g(\mu)\,h(\phi)$, the unbiased source distribution may be written

$$J(E,\vec{\Omega}) = \frac{\psi(E_{\min}) - \psi(E_{\max})}{4}\, f(E)\, g(\mu)\, h(\phi)\,, \tag{6}$$

where

$$\begin{aligned}
\frac{\psi(E_{\min}) - \psi(E_{\max})}{4} &= W_o = \text{the initial weight assigned to each source particle,} \\
f(E) &= \text{the pdf in energy} = \frac{\Phi(E)}{\psi(E_{\min}) - \psi(E_{\max})}, \\
g(\mu) &= \text{the pdf in polar angle} = 2\mu, \\
h(\phi) &= \text{the pdf in azimuthal angle} = (2\pi)^{-1}.
\end{aligned}$$

To improve the statistical fluctuations in the dose distributions in the electronics and sensitive areas, the source particle energies and directions were not sampled from the pdf's given above but instead were sampled from biased distributions. These biased distributions were constructed so that those source-particle energies and directions that resulted in relatively large dose contributions were sampled more frequently. Statistical weighting fractions to account for the biasing were then applied to each source particle so that the original incident source spectral shape and normalization are preserved. For the energy biasing, the energy intervals, ΔE, and the sampling fractions for each energy interval used, P_E, are summarized in Table 8 for Van Allen belt, and nuclear enhanced electron spectra. The particle energy was selected uniformly within each energy interval according to the relation

$$E_S = E_U - R(E_U - E_L) = E_U - R(\Delta E)\,, \tag{7}$$

where

$E_S =$ the sample energy,

$E_U, E_L =$ the upper and lower bounds, respectively, of the energy interval in which the sample is taken, and

$R =$ a random number between 0 and 1.

The biased pdf in energy is now given by

$$f^*(E) = \frac{P_E}{\Delta E}\,, \tag{8}$$

and Eq. (6) may be rewritten as

Table 8

Energy Intervals and Sampling Fractions for Source Particle Biasing in the HETC and EGS4 Calculations

Energy Interval (MeV)	Sampling Fraction (p_E)
Van Allen Belt Proton Spectra	
30–40	0.10
40–50	0.13
50–100	0.35
100–200	0.25
200–400	0.12
400–1000	0.05
Background Van Allen Belt Electron Spectra	
0.05–0.1	0.02
0.1–0.5	0.02
0.5–1.0	0.03
1.0–1.5	0.04
1.5–2.0	0.06
2.0–2.5	0.08
2.5–3.0	0.10
3.0–3.5	0.15
3.5–4.0	0.20
4.0–4.6	0.30
Nuclear Enhanced Electron Spectra	
0.04–0.25	0.02
0.25–0.5	0.02
0.5–1.0	0.03
1.0–2.0	0.04
2.0–3.0	0.06
3.0–4.0	0.08
4.0–5.0	0.10
5.0–6.0	0.15
6.0–7.0	0.20
7.0–10.0	0.30

$$J(E,\bar{\Omega}) = W_o \left[\frac{f(E)}{f^*(E)}\right] f^*(E)\, g(\mu)\, h(\phi)\,. \tag{9}$$

where

$$\left[\frac{f(E)}{f^*(E)}\right] = W_E = \text{the weight factor due energy biasing}\,.$$

then

$$J(E,\vec{\Omega}) = W_o\, W_E\, f^*(E)\, g(\mu)\, h(\phi)\,. \tag{10}$$

Angular biasing of the incident spectra was accomplished using similar techniques. The angular intervals, $\Delta\mu$, and the sampling fractions, p_μ, for samples within various solid angles are summarized in Table 9.

Table 9

Angular Intervals and Sampling Fractions for Source Particle Biasing in the HETC and EGS4 Calculations

Angular Interval[a]	Sampling Fraction (p_u)
0.0– 5.0	0.12375
5.0–10.0	0.12375
10.0–15.0	0.12375
15.0–20.0	0.12375
20.0–25.0	0.12375
25.0–30.0	0.12375
30.0–35.0	0.12375
35.0–40.0	0.12375
40.0–90.0	0.01000

[a]Angles listed in degrees (θ)

Particles were selected uniformly within each angular interval according to the formula

$$\mu' = \mu_j - R(\mu_j - \mu_{j+1}) = \mu_j - R\,\Delta\mu\,. \tag{11}$$

The biased pdf in polar angle can now be written

$$g^*(\mu) = \frac{P_\mu}{\Delta\mu},$$

and Eq. (9) may be written

$$J(E,\bar{\Omega}) = W_o\, W_E\, W_\mu\, f^*(E)\, g^*(\mu)\, h(\phi)\,, \tag{12}$$

where

$$W_\mu = \left[\frac{g(\mu)}{g^*(\mu)}\right] = \left[\frac{2\mu\Delta\mu}{p_\mu}\right] = \text{the weight factor due to direction biasing interval } \Delta\mu \text{ about } \mu.$$

Since all source particles were uniformly sampled in the azimuthal angles, $h^*(\phi) = h(\phi)$.

3.2 DETECTOR LOCATIONS

The radiation damage in the SBI and the KKVs was estimated at 68 different locations that were considered to be potentially most sensitive to the natural and enhanced VAB radiation. The locations of the detectors used in this and complementary studies[10,11,12] are given in Table 10. In the context of this study, the term detector refers to a region in the combinatorial geometry representation of the SBI platform and the KKVs in which an estimate of the radiation damage is desired. For example, the C^3 bay (see Figure 3), contains fifteen detector regions; the central critical electronics component box, six angular segments in the inner ring, and eight segments in the outer ring. Dividing the inner and outer rings into angularly segmented detector regions was done to determine the variations in the damage from inherent shielding of the various regions by components inside the platform. While this is not a strong requirement for this analysis where the incident radiation is isotropic, it is essential for those studies where the radiation may be directional.

Separate detector regions were adopted for the SBI fuel tanks, antenna, solar panels, and the KKV fuel tanks, computers, and sensors. The platform fuel tank was taken to be one hydrazine filled region. Each solar panel and the antenna was treated using five detector regions. Each KKV fuel tank, computer and sensor bay was taken to be a separate detector region.

The solar panel detector regions were selected to provide sufficient data to estimate the effects of surface degradation by incident VAB radiation and to also have the capability for predicting blowoff, melting, etc., of material from short duration pulsed radiation from nuclear weapon detonations in the vicinity of the platform.

Table 10

The Detector Regions Implemented in the Radiation Transport Analysis Routines

SBI Platform Component	Detector Region
C^3 Bay Critical Components Central Instrument Box	1
C^3 Bay Inner Instrument Ring	
0 to 60 Degree Segment	2
60 to 120 Degree Segment	3
120 to 180 Degree Segment	4
180 to 240 Degree Segment	5
240 to 300 Degree Segment	6
300 to 360 Degree Segment.	7
C^3 Bay Outer Instrument Ring	
0 to 45 Degree Segment	8
45 to 90 Degree Segment	9
90 to 135 Degree Segment	10
135 to 180 Degree Segment	11
180 to 225 Degree Segment	12
225 to 270 Degree Segment	13
270 to 315 Degree Segment	14
315 to 360 Degree Segment	15
Kinetic Kill Vehicle Computers	
KKV Number 1	16
KKV Number 2	17
KKV Number 3	18
KKV Number 4	19
KKV Number 5	20
KKV Number 6	21
KKV Number 7	22
KKV Number 8	23
KKV Number 9	24
KKV Number 10	25
Kinetic Kill Vehicle Sensors	
KKV Number 1	26
KKV Number 2	27
KKV Number 3	28
KKV Number 4	29
KKV Number 5	30
KKV Number 6	31
KKV Number 7	32
KKV Number 8	33
KKV Number 9	34
KKV Number 10	35

Table 10 (Continued)

SBI Platform Component	Detector Region
Right Solar Panel	
Inner 0.5 cm Thick Shell	36
Next 0.5 cm Thick Shell	37
Next 0.5 cm Thick Shell	38
Next 0.5 cm Thick Shell	39
Outer 0.5 cm Thick Shell	40
Left Solar Panel	
Inner 0.5 cm Thick Shell	41
Next 0.5 cm Thick Shell	42
Next 0.5 cm Thick Shell	43
Next 0.5 cm Thick Shell	44
Outer 0.5 cm Thick Shell	45
BSTS, SSTS Antenna	
Inner 1.0 cm Thick Shell	46
Next 1.0 cm Thick Shell	47
Next 1.0 cm Thick Shell	48
Next 1.0 cm Thick Shell	49
Outer 1.0 cm Thick Shell	50
Kinetic Kill Vehicle Rocket Fuel Tanks	
KKV Number 1	51
KKV Number 2	52
KKV Number 3	53
KKV Number 4	54
KKV Number 5	55
KKV Number 6	56
KKV Number 7	57
KKV Number 8	58
KKV Number 9	59
KKV Number 10	60
SBI Weapon Platform Rocket Fuel Tanks	
SBI Tank Number 1	61
SBI Tank Number 2	62
SBI Tank Number 3	63
SBI Tank Number 4	64
SBI Tank Number 5	65
SBI Tank Number 6	66
SBI Tank Number 7	67
SBI Tank Number 8	68

ORNL-DWG 88Z-14290R

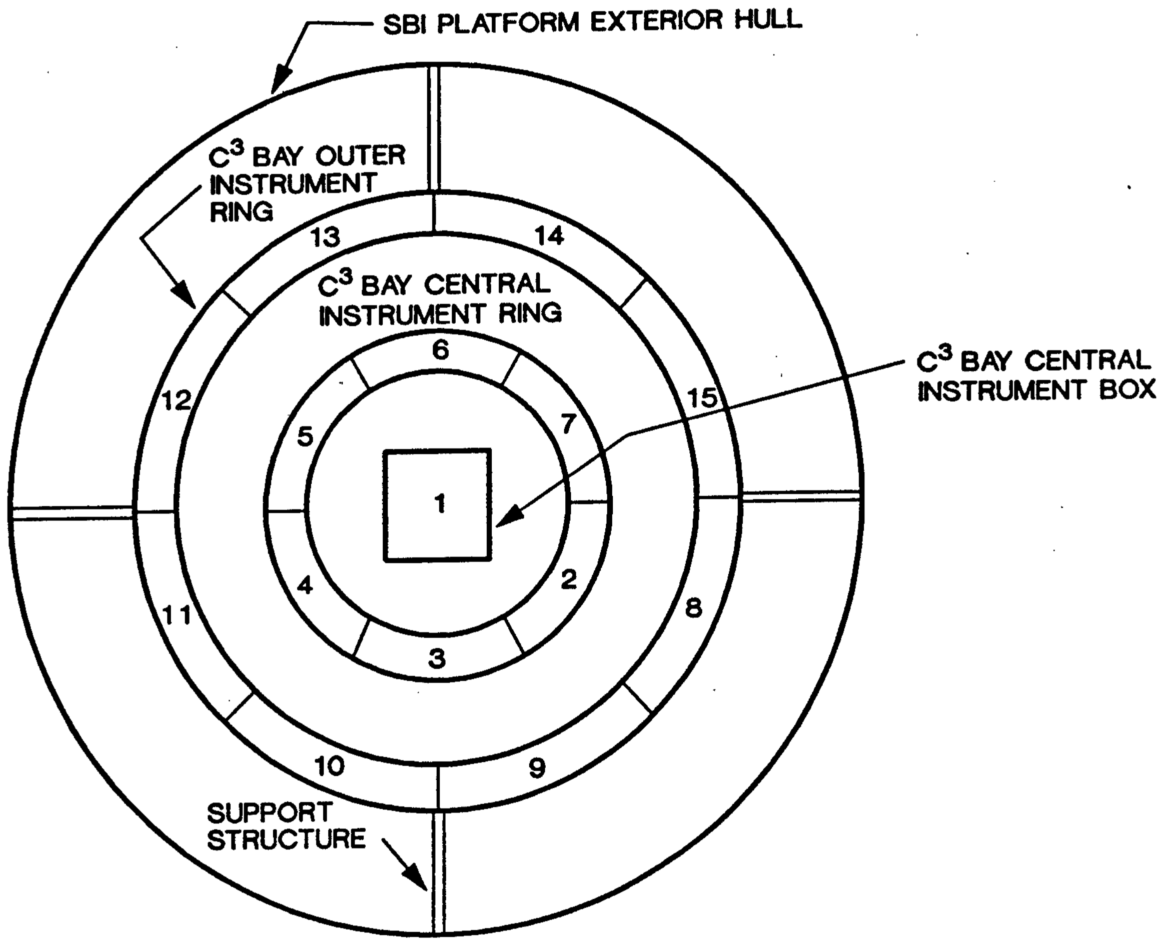

Figure 3. Schematic diagram of the Space Based Interceptor Weapon Platform Command, Control, Communications (C^3) Bay detailing the detector region numbering system used in the radiation transport analysis.

4. RESULTS

4.1 RADIATION DAMAGE FROM VAN ALLEN BELT PROTONS

The radiation damage in the various components of the SBI platform and KKVs from VAB proton radiation for the source spectrum given in Table 4 is summarized in Table 11. The column labeled "Primary" gives the dose due to the incident proton radiation only. The column labeled "Primary Plus Secondary" is the dose from the incident protons plus the dose from secondary particles produced by the reactions of the incident radiation in the materials of the system. The secondary radiation transport calculation was not carried out for particle energies below 20 MeV. Since the contribution from secondary radiation was, in general, small, it was concluded that the impact of low energy particles would also be minimal.

The dose/day from VAB protons in all 68 detector regions is low. Even after ten years exposure to this radiation (see Table 12), the cumulative doses range from approximately 200 rads in the C^3 bay to 1500 rads in the inner layers of the solar panel. These doses are well below the total dose levels (10^6 rad) at which silicon based electronics and solar cells will fail.

4.2 RADIATION DAMAGE FROM VAN ALLEN BELT ELECTRONS (NATURAL AND ENHANCED)

The damage from VAB electrons and enhanced electron belt radiation in the SBI platform and KKVs at an altitude of 500 km is given in Tables 13 and 14, respectively. The damage from natural radiation is normalized to rads/day whereas the enhanced damage is in units of rads/electron.

The enhanced electron spectra showed small (less than 5%) spectral differences with respect to orbital height, orbital inclination, and time after nuclear detonation (6 hours to 1 year). Therefore, the spectrum was averaged and the total electron fluence as a function of time after the nuclear detonation was used to determine the dose due to the nuclear enhanced electron radiation environment. The electron fluence at an altitude of 500 kilometers from a high altitude nuclear detonation as a function of time after detonation is given in Table 7. Multiplying the normalized doses given in Table 14 by the total electron fluences given in Table 7 yields the cumulative doses due to the nuclear enhanced electron environment as a function of time after nuclear detonation. The cumulative doses are presented in Table 15.

Two trends are evident in the data presented in Tables 13 and 14. First is the dose as a function of depth in the solar panels and the antenna. The low energy natural electron spectrum results predominately in a surface dose in the components. The dose then falls off rapidly with depth. Any damage to components inside of the platform can result only from secondary bremsstrahlung photons produced from primary electron interactions. The enhanced electron spectrum also leads to a large surface dose. However, since the electrons are somewhat more energetic and the spectrum is harder, the dose profile in these components is much flatter and the dose in the interior layers is significantly higher than the dose due to the natural

Table 11

Dose Due to Van Allen Belt Protons for a Circular Orbit at an Altitude of 500 Kilometers

Detector Region	Primary[a] (rads/day)	Primary & Secondary[b] (rads/day)
C^3 Bay Central Instrument Box	4.74−02 ± 10%	4.89−02[c] ± 16%
C^3 Bay Inner Instrument Ring	4.90−02 ± 3%	4.34−02 ± 4%
C^3 Bay Outer Instrument Ring	6.89−02 ± 3%	6.26−02 ± 3%
Average for the Kinetic Kill Vehicle Computers	6.28−02 ± 4%	6.61−02 ± 5%
Average for the Kinetic Kill Vehicle Sensors	7.63−02 ± 3%	7.07−02 ± 4%
Inner 0.5 cm Thickness of the Solar Panels	4.14−01 ± 2%	4.10−01 ± 2%
Next 0.5 cm Thickness of the Solar Panels	1.75−01 ± 3%	1.71−01 ± 4%
Next 0.5 cm Thickness of the Solar Panels	2.12−01 ± 3%	2.01−01 ± 3%
Next 0.5 cm Thickness of the Solar Panels	2.39−01 ± 2%	2.43−01 ± 2%
Outer 0.5 cm Thickness of the Solar Panels	1.05−01 ± 3%	1.17−01 ± 4%
Average for the Solar Panels	1.85−01 ± 1%	2.13−01 ± 1%
Inner 1.0 cm Thickness of the BSTS, SSTS Antenna	3.22−01 ± 6%	3.30−01 ± 12%
Next 1.0 cm Thickness of the BSTS, SSTS Antenna	1.51−01 ± 13%	1.57−01 ± 17%
Next 1.0 cm Thickness of the BSTS, SSTS Antenna	2.13−01 ± 10%	1.97−01 ± 9%
Next 1.0 cm Thickness of the BSTS, SSTS Antenna	2.04−01 ± 8%	2.29−01 ± 8%
Outer 1.0 cm Thickness of the BSTS, SSTS Antenna	1.22−01 ± 13%	1.12−01 ± 10%
Average for the BSTS, SSTS Antenna	1.96−01 ± 4%	1.64−01 ± 5%
Average for the Kinetic Kill Vehicle Rocket Fuel	7.94−02 ± 2%	7.31−02 ± 3%
Average for the SBI Weapon Platform Rocket Fuel	6.85−02 ± 2%	6.42−02 ± 2%

[a] Dose due to unattenuated primary protons only.
[b] Dose due to primary and secondary collisions and full proton transport.
[c] Read as 4.89×10^{-2}.

Table 12

Cumulative Dose After Ten Years Due to Van Allen Belt Protons for a Circular Orbit at an Altitude of 500 Kilometers

Detector Region	Primary[a] (rads)	Primary & Secondary[b] (rads)
C^3 Bay Central Instrument Box	1.73+02 ± 10%	1.79+02[c] ± 16%
C^3 Bay Inner Instrument Ring	1.79+02 ± 3%	1.59+02 ± 4%
C^3 Bay Outer Instrument Ring	2.52+02 ± 3%	2.29+02 ± 3%
Average for the Kinetic Kill Vehicle Computers	2.29+02 ± 4%	2.41+02 ± 5%
Average for the Kinetic Kill Vehicle Sensors	2.79+02 ± 3%	2.58+02 ± 4%
Inner 0.5 cm Thickness of the Solar Panels	1.51+03 ± 2%	1.50+03 ± 2%
Next 0.5 cm Thickness of the Solar Panels	6.39+02 ± 3%	6.25+02 ± 4%
Next 0.5 cm Thickness of the Solar Panels	7.74+02 ± 3%	7.34+02 ± 3%
Next 0.5 cm Thickness of the Solar Panels	8.73+02 ± 2%	8.88+02 ± 2%
Outer 0.5 cm Thickness of the Solar Panels	3.84+02 ± 3%	4.27+02 ± 4%
Average for the Solar Panels	6.76+02 ± 1%	7.78+02 ± 1%
Inner 1.0 cm Thickness of the BSTS, SSTS Antenna	1.18+03 ± 6%	1.21+03 ± 12%
Next 1.0 cm Thickness of the BSTS, SSTS Antenna	5.52+02 ± 13%	5.73+02 ± 17%
Next 1.0 cm Thickness of the BSTS, SSTS Antenna	7.78+02 ± 10%	7.20+02 ± 9%
Next 1.0 cm Thickness of the BSTS, SSTS Antenna	7.45+02 ± 8%	8.36+02 ± 8%
Outer 1.0 cm Thickness of the BSTS, SSTS Antenna	4.46+02 ± 13%	4.09+02 ± 10%
Average for the BSTS, SSTS Antenna	7.16+02 ± 4%	5.99+02 ± 5%
Average for the Kinetic Kill Vehicle Rocket Fuel	2.90+02 ± 2%	2.67+02 ± 3%
Average for the SBI Weapon Platform Rocket Fuel	2.50+02 ± 2%	2.34+02 ± 2%

[a] Dose due to unattenuated primary protons only.

[b] Dose due to primary and secondary collisions and full proton transport.

[c] Read as 1.79×10^2.

Table 13

Dose Due to Natural Background Van Allen Belt Electrons for a Circular Orbit at an Altitude of 500 Kilometers

Detector Region	Natural Background Dose (rads/day)	Natural Background Dose After Ten Years (rads)
C^3 Bay Central Instrument Box	3.23−05[a] ± 30%	1.18−01 ± 30%
C^3 Bay Inner Instrument Ring	5.19−05 ± 15%	1.90−01 ± 15%
C^3 Bay Outer Instrument Ring	1.49−04 ± 12%	5.44−01 ± 12%
Average for the Kinetic Kill Vehicle Computers	7.39−05 ± 15%	2.70−01 ± 15%
Average for the Kinetic Kill Vehicle Sensors	1.20−04 ± 11%	4.38−01 ± 11%
Inner 0.5 cm Thickness of the Solar Panels	5.71−04 ± 14%	2.09+00 ± 14%
Next 0.5 cm Thickness of the Solar Panels	3.25−03 ± 3%	1.19+00 ± 3%
Next 0.5 cm Thickness of the Solar Panels	3.10−02 ± 2%	1.13+02 ± 2%
Next 0.5 cm Thickness of the Solar Panels	2.26−01 ± 2%	8.25+02 ± 2%
Outer 0.5 cm Thickness of the Solar Panels	8.78+00 ± 2%	3.21+04 ± 2%
Average for the Solar Panels	2.29−03 ± 3%	8.36+00 ± 3%
Inner 1.0 cm Thickness of the BSTS, SSTS Antenna	5.17−04 ± 33%	1.89+00 ± 33%
Next 1.0 cm Thickness of the BSTS, SSTS Antenna	4.19−04 ± 26%	1.53+00 ± 26%
Next 1.0 cm Thickness of the BSTS, SSTS Antenna	5.87−03 ± 12%	2.14+01 ± 12%
Next 1.0 cm Thickness of the BSTS, SSTS Antenna	7.29−02 ± 6%	2.66+02 ± 6%
Outer 1.0 cm Thickness of the BSTS, SSTS Antenna	6.23+00 ± 10%	2.28+04 ± 10%
Average for the BSTS, SSTS Antenna	5.83−04 ± 2%	2.13+00 ± 2%
Average for the Kinetic Kill Vehicle Rocket Fuel	1.02−04 ± 11%	3.73−01 ± 11%
Average for the SBI Weapon Platform Rocket Fuel	3.51−04 ± 7%	1.28+00 ± 7%

[a] Read as 3.23×10^{-5}.

Table 14

Dose Due to Nuclear Enhanced Van Allen Belt Electrons from a High-Altitude Nuclear Burst for a Circular Orbit at an Altitude of 500 Kilometers

Detector Region	Normalized Trapped Dose[a] (rads·cm^2/electron)
C^3 Bay Central Instrument Box	1.13−12[b] ± 26%
C^3 Bay Inner Instrument Ring	3.79−12 ± 11%
C^3 Bay Outer Instrument Ring	6.85−12 ± 6%
Average for the Kinetic Kill Vehicle Computers	4.12−12 ± 9%
Average for the Kinetic Kill Vehicle Sensors	6.42−12 ± 7%
Inner 0.5 cm Thickness of the Solar Panels	2.65−10 ± 2%
Next 0.5 cm Thickness of the Solar Panels	5.66−10 ± 2%
Next 0.5 cm Thickness of the Solar Panels	1.50−09 ± 2%
Next 0.5 cm Thickness of the Solar Panels	3.99−09 ± 2%
Outer 0.5 cm Thickness of the Solar Panels	9.79−09 ± 1%
Average for the Solar Panels	3.58−10 ± 1%
Inner 1.0 cm Thickness of the BSTS, SSTS Antenna	6.83−11 ± 8%
Next 1.0 cm Thickness of the BSTS, SSTS Antenna	1.60−10 ± 11%
Next 1.0 cm Thickness of the BSTS, SSTS Antenna	4.85−10 ± 10%
Next 1.0 cm Thickness of the BSTS, SSTS Antenna	1.78−10 ± 7%
Outer 1.0 cm Thickness of the BSTS, SSTS Antenna	7.76−09 ± 4%
Average for the BSTS, SSTS Antenna	8.64−11 ± 6%
Average for the Kinetic Kill Vehicle Rocket Fuel	5.22−12 ± 5%
Average for the SBI Weapon Platform Rocket Fuel	1.52−11 ± 4%

[a]Excludes natural background electron dose.
[b]Read as 1.13×10^{-12}.

Table 15

Cumulative Dose Due to Nuclear Enhanced Van Allen Belt Electrons from a High-Altitude Nuclear Burst for a Circular Orbit at an Altitude of 500 Kilometers

Detector Region	Cumulative Dose After High Altitude Nuclear Weapon Burst[a] (rads)							
	6 Hrs	1 Day	2 Days	7 Days	30 Days	60 Days	180 Days	1 Year
C^3 Bay Central Instrument Box	8.80−01[b]	2.73+00	5.17+00	1.43+01	3.50+01	5.50+01	1.08+02	1.60+02
C^3 Bay Inner Instrument Ring	2.95+00	9.16+00	1.73+01	4.80+01	1.17+02	1.85+02	3.62+02	5.38+02
C^3 Bay Outer Instrument Ring	5.34+00	1.66+01	3.14+01	8.69+01	2.12+02	3.34+02	6.55+02	9.74+02
Average for the Kinetic Kill Vehicle Computers	3.21+00	9.97+00	1.89+01	5.22+01	1.28+02	2.01+02	3.94+02	5.86+02
Average for the Kinetic Kill Vehicle Sensors	5.00+00	1.55+01	2.94+01	8.14+01	1.99+02	3.13+02	6.13+02	9.12+02
Inner 0.5 cm Thickness of the Solar Panels	2.07+02	6.41+02	1.21+03	3.36+03	8.21+03	1.29+04	2.53+04	3.77+04
Next 0.5 cm Thickness of the Solar Panels	4.41+02	1.37+03	2.59+03	7.17+03	1.75+04	2.76+04	5.41+04	8.04+04
Next 0.5 cm Thickness of the Solar Panels	1.17+03	3.64+03	6.89+03	1.91+04	4.67+04	7.34+04	1.44+05	2.14+05
Next 0.5 cm Thickness of the Solar Panels	3.12+03	9.67+03	1.83+04	5.06+04	1.24+05	1.95+05	3.82+05	5.68+05
Outer 0.5 cm Thickness of the Solar Panels	7.64+03	2.37+04	4.49+04	1.24+05	3.04+05	4.78+05	9.36+05	1.39+06
Average for the Solar Panels	2.79+02	8.67+02	1.64+03	4.54+03	1.11+04	1.75+04	3.43+04	5.09+04
Inner 1.0 cm Thickness of the BSTS, SSTS Antennna	5.33+01	1.65+02	3.13+02	8.67+02	2.12+03	3.34+03	6.53+03	9.72+03
Next 1.0 cm Thickness of the BSTS, SSTS Antenna	1.25+02	3.87+02	7.33+02	2.03+03	4.96+03	7.81+03	1.53+04	2.28+04
Next 1.0 cm Thickness of the BSTS, SSTS Antenna	3.78+02	1.17+03	2.22+03	6.15+03	1.50+04	2.37+04	4.64+04	6.90+04
Next 1.0 cm Thickness of the BSTS, SSTS Antenna	1.39+03	4.32+03	8.17+03	2.26+04	5.53+04	8.71+04	1.71+05	2.54+05
Outer 1.0 cm Thickness of the BSTS, SSTS Antenna	6.05+03	1.88+04	3.55+04	9.84+04	2.41+05	3.79+05	7.42+05	1.10+06
Average for the BSTS, SSTS Antenna	6.74+01	2.09+02	3.95+02	1.09+03	2.68+03	4.21+03	8.26+03	1.23+04
Average for the Kinetic Kill Vehicle Rocket Fuel	4.07+00	1.26+01	2.39+01	6.62+01	1.62+02	2.55+02	4.99+02	7.42+02
Average for the SBI Weapon Platform Rocket Fuel	1.19+01	3.68+01	6.96+01	1.93+02	4.71+02	7.42+02	1.45+03	2.16+03

[a]Excludes natural background electron dose.

[b]Read as 8.80×10^{-1}.

electron environment. The second trend is the magnitude of the dose produced by the two radiation modes. Comparing the dose averaged through the solar panel reveals that the dose rate from the natural environment is 2.29×10^{-3} rad/day whereas the enhanced electron dose rate at six hours after weapon detonation is 1.1×10^{3} rads/day. The slow decay of the enhanced spectrum indicates that the dose accumulated in the outer layers of the solar panels and antenna is sufficiently large to cause material damage and bit upset, degradation, and failure in near surface mounted electronic components.

To determine the combined dose from both environments, the dose rate from the natural environment must be multiplied by the time that the platform resided in the environment and added to the cumulative dose from enhancement. For example, if the platform was in orbit for one year prior to the detonation of a weapon in space, the dose average with depth in the solar panels would be 0.84 rads from natural electrons and 67.5 rads from protons. Six hours after the explosion, the dose from enhanced electrons would be 279 rads.

5. CONCLUSIONS

The calculated results presented here show that the ORNL SBI platform will survive long term (10 years) exposure to VAB protons and electrons at 500 km orbit altitudes. The radiation damage in all components including the exposed solar panels and antenna are well below damage levels. However, the situation is much different when the electron belts are enhanced by the detonation of a nuclear weapon in space. Multiple weapon detonations will increase these doses (see Section 4.2). The higher intensity and harder electron spectrum will lead to more rapid and severe damage in exposed components and those mounted on or near the surface of the platform.

The ORNL platform, though similar to an actual design, may still be sufficiently different that the damage levels to components mounted inside of the platform will be more severe than reported here. Also, in these calculations, the electronics were treated as homogenized silicon with the material density tailored to account for distribution in the circuit. Calculation of the damage in more realistic configurations may result in more severe damage because of lighter, thinner, and lower density materials used in the platform.

6. ACKNOWLEDGEMENTS

The authors wish to thank Mrs. Dawn C. Human for her significant efforts in typing this manuscript and for her assistance throughout this program.

APPENDIX A

Combinatorial Geometry Input for the SBI Weapon Platform and Kinetic Kill Vehicles.

```
 0    0                       KKV PLATFORM GEOMETRY
                                                                   EXT VOID
SPH          0.0       0.0       0.0     1000.0                    GLOBE
SPH          0.0       0.0       0.0      525.0
RCC          0.0       0.0    +15.240       0.0        0.0    198.12PLTFRM EX
            81.60
RCC          0.0       0.0    +15.240       0.0        0.0    197.80PLTFRM LN
            81.28
RCC          0.0       0.0     -15.24       0.0        0.0     30.48INSTR BAY
            81.60
RCC          0.0       0.0     -14.92       0.0        0.0     29.84 I.B. LNR
            81.28
RCC          0.0       0.0     -14.92       0.0        0.0     29.84
            55.00
RCC          0.0       0.0     -14.92       0.0        0.0     29.84
            54.68
RCC          0.0       0.0     -14.92       0.0        0.0     29.84
            40.32
RCC          0.0       0.0     -14.92       0.0        0.0     29.84
            40.00
RCC          0.0       0.0     -14.92       0.0        0.0     29.84
            35.00
RCC          0.0       0.0     -14.92       0.0        0.0     29.84
            34.68
RCC          0.0       0.0     -14.92       0.0        0.0     29.84
            25.32
RCC          0.0       0.0     -14.92       0.0        0.0     29.84
            25.00
BOX          7.50     -7.50    -14.92    -15.00        0.0       0.0 OUTER BX
             0.0      15.00      0.0        0.0        0.0     29.84
BOX          7.18     -7.18    -14.60    -14.36        0.0       0.0 INNER BX
             0.0      14.36      0.0        0.0        0.0     29.20
BOX         81.28     -0.16    -12.00    -26.28        0.0       0.0 SPPRT B1
             0.0       0.32      0.0        0.0        0.0     24.00
BOX         -0.16     81.28    -12.0       0.32        0.0       0.0 SPPRT B2
             0.0     -26.28      0.0        0.0        0.0     24.00
BOX        -81.28      0.16    -12.0      26.28        0.0       0.0 SPPRT B3
             0.0      -0.32      0.0        0.0        0.0     24.00
BOX         -0.16    -81.28    -12.0       0.32        0.0       0.0 SPPRT B4
             0.0      26.28      0.0        0.0        0.0     24.00
RCC         50.8       0.0      15.24       0.0        0.0    198.12 FOT 1
            20.64
RCC         50.8       0.0      15.24       0.0        0.0    198.12 FIT 1
            20.32
RCC         35.92     35.92     15.24       0.0        0.0    198.12 FOT 2
            10.48
RCC         35.92     35.92     15.24       0.0        0.0    197.8  FIT 2
            10.16
```

```
RCC     0.0       50.8     15.24    0.0    0.0    198.12 FOT 3
        20.64
RCC     0.0       50.8     15.24    0.0    0.0    198.12 FIT 3
        20.32
RCC     -35.92    35.92    15.24    0.0    0.0    198.12 FOT 4
        10.48
RCC     -35.92    35.92    15.24    0.0    0.0    197.80 FIT 4
        10.16
RCC     -50.80    0.0      15.24    0.0    0.0    198.12 FOT 5
        20.64
RCC     -50.80    0.0      15.24    0.0    0.0    198.12 FIT 5
        20.32
RCC     -35.92    -35.92   15.24    0.0    0.0    198.12 FOT 6
        10.48
RCC     -35.92    -35.92   15.24    0.0    0.0    197.80 FIT 6
        10.16
RCC     0.0       -50.80   15.24    0.0    0.0    198.12 FOT 7
        20.64
RCC     0.0       -50.80   15.24    0.0    0.0    198.12 FIT 7
        20.32
RCC     35.92     -35.92   15.24    0.0    0.0    198.12 FOT 8
        10.48
RCC     35.92     -35.92   15.24    0.0    0.0    197.80 FIT 8
        10.16
RCC     0.0       0.0      15.24    0.0    0.0    198.12 FOT 9
        20.64
RCC     0.0       0.0      15.24    0.0    0.0    198.12 FIT 9
        20.32
RCC     50.8      0.0      -15.24   0.0    0.0    -198.12 BOT 1
        20.64
RCC     50.8      0.0      -15.24   0.0    0.0    -198.12 BIT 1
        20.32
RCC     35.92     35.92    -15.24   0.0    0.0    -198.12 BOT 2
        10.48
RCC     35.92     35.92    -15.24   0.0    0.0    -197.8  BIT 2
        10.16
RCC     0.0       50.8     -15.24   0.0    0.0    -198.12 BOT 3
        20.64
RCC     0.0       50.8     -15.24   0.0    0.0    -198.12 BIT 3
        20.32
RCC     -35.92    35.92    -15.24   0.0    0.0    -198.12 BOT 4
        10.48
RCC     -35.92    35.92    -15.24   0.0    0.0    -197.80 BIT 4
        10.16
RCC     -50.80    0.0      -15.24   0.0    0.0    -198.12 BOT 5
        20.64
RCC     -50.80    0.0      -15.24   0.0    0.0    -198.12 BIT 5
        20.32
RCC     -35.92    -35.92   -15.24   0.0    0.0    -198.12 BOT 6
        10.48
RCC     -35.92    -35.92   -15.24   0.0    0.0    -197.80 BIT 6
        10.16
RCC     0.0       -50.80   -15.24   0.0    0.0    -198.12 BOT 7
        20.64
```

RCC	0.0	-50.80	-15.24	0.0	0.0	-198.12	BIT 7
	20.32						
RCC	35.92	-35.92	-15.24	0.0	0.0	-198.12	BOT 8
	10.48						
RCC	35.92	-35.92	-15.24	0.0	0.0	-197.80	BIT 8
	10.16						
RCC	0.0	0.0	-15.24	0.0	0.0	-198.12	BOT 9
	20.64						
RCC	0.0	0.0	-15.24	0.0	0.0	-198.12	BIT 9
	20.32						
BOX	20.64	-0.16	15.24	60.74	0.0	0.0	FSB 1
	0.0	0.32	0.0	0.0	0.0	197.80	
BOX	14.71	14.48	15.24	42.88	42.88	0.0	FSB 2
	-0.226	.226	0.0	0.0	0.0	197.80	
BOX	-0.16	20.64	15.24	0.32	0.0	0.0	FSB 3
	00.00	60.74	0.0	0.0	0.0	197.80	
BOX	14.48	14.71	15.24	-42.88	42.88	0.0	FBS 4
	-0.226	-0.226	0.0	0.0	0.0	197.80	
BOX	-20.64	0.16	15.24	-60.74	0.0	0.0	FBS 5
	0.0	-0.320	0.0	0.0	0.0	197.80	
BOX	-14.71	-14.48	15.24	-42.88	-42.88	0.0	FBS 6
	0.226	-0.226	0.0	0.0	0.0	197.80	
BOX	0.16	-20.64	15.24	-0.32	0.0	0.0	FBS 7
	000.00	-60.74	0.0	0.0	0.0	197.80	
BOX	14.48	14.71	15.24	42.88	-42.88	0.0	FBS 8
	0.226	0.226	0.0	0.0	0.0	197.80	
BOX	20.64	-0.16	-15.24	60.74	0.0	0.0	BSB 1
	0.0	0.32	0.0	0.0	0.0	-197.80	
BOX	14.71	14.48	-15.24	42.88	42.88	0.0	BSB 2
	-0.226	.226	0.0	0.0	0.0	-197.80	
BOX	-0.16	20.64	-15.24	0.32	0.0	0.0	BSB 3
	00.00	60.74	0.0	0.0	0.0	-197.80	
BOX	14.48	14.71	-15.24	-42.88	42.88	0.0	BSB 4
	-0.226	-0.226	0.0	0.0	0.0	-197.80	
BOX	-20.64	0.16	-15.24	-60.74	0.0	0.0	BSB 5
	0.0	-0.320	0.0	0.0	0.0	-197.80	
BOX	-14.71	-14.48	-15.24	-42.88	-42.88	0.0	BSB 6
	0.226	-0.226	0.0	0.0	0.0	-197.80	
BOX	0.16	-20.64	-15.24	-0.32	0.0	0.0	BSB 7
	000.00	-60.74	0.0	0.0	0.0	-197.80	
BOX	14.48	14.71	-15.24	42.88	-42.88	0.0	BSB 8
	0.226	0.226	0.0	0.0	0.0	-197.80	
RCC	50.8	0.0	213.36	0.0	0.0	0.32	FTC 1
	20.64						
RCC	0.0	50.8	213.36	0.0	0.0	0.32	FTC 3
	20.64						
RCC	-50.80	0.0	213.36	0.0	0.0	0.32	FTC 5
	20.64						
RCC	0.0	-50.8	213.36	0.0	0.0	0.32	FTC 7
	20.64						
RCC	0.0	0.0	213.36	0.0	0.0	0.32	FTC 9
	20.64						
RCC	50.8	0.0	-213.36	0.0	0.0	-0.32	BTC 1
	20.64						

RCC	0.0	50.8	-213.36	0.0	0.0	-0.32	BTC 3
	20.64						
RCC	-50.80	0.0	-213.36	0.0	0.0	-0.32	BTC 5
	20.64						
RCC	0.0	-50.8	-213.36	0.0	0.0	-0.32	BTC 7
	20.64						
RCC	0.0	0.0	-213.36	0.0	0.0	-0.32	BTC 9
	20.64						
TRC	50.80	.00	22.86	.00	.00	30.48	NOZZLE
	20.00	14.0					
TRC	50.80	.00	22.86	.00	.00	30.48	
	19.68	13.68					
RCC	50.80	.00	53.34	.00	.00	15.24	MOTOR
	14.00						
RCC	50.80	.00	53.66	.00	.00	14.92	
	13.68						
RCC	50.80	.00	68.58	.00	.00	45.72	FUEL TANK
	20.00						
RCC	50.80	.00	68.90	.00	.00	45.08	
	19.68						
RCC	50.80	.00	114.30	.00	.00	30.48	COMPUTR
	14.00						
RCC	50.80	.00	114.62	.00	.00	29.84	
	13.68						
RCC	50.80	.00	114.62	.00	.00	29.84	
	10.68						
RCC	50.80	.00	114.62	.00	.00	29.84	
	3.68						
RCC	50.80	.00	144.78	.00	.00	30.48	SENSORS
	20.00						
RCC	50.80	.00	145.10	.00	.00	29.84	
	19.68						
RCC	50.80	.00	145.10	.00	.00	29.84	
	15.68						
RCC	50.80	.00	145.10	.00	.00	29.84	
	5.68						
RCC	50.80	.00	175.26	.00	.00	18.64	HEAD
	4.66						
TRC	.00	50.80	22.86	.00	.00	30.48	NOZZLE
	20.00	14.0					
TRC	.00	50.80	22.86	.00	.00	30.48	
	19.68	13.68					
RCC	.00	50.80	53.34	.00	.00	15.24	MOTOR
	14.00						
RCC	.00	50.80	53.66	.00	.00	14.92	
	13.68						
RCC	.00	50.80	68.58	.00	.00	45.72	FUEL TANK
	20.00						
RCC	.00	50.80	68.90	.00	.00	45.08	
	19.68						
RCC	.00	50.80	114.30	.00	.00	30.48	COMPUTR
	14.00						
RCC	.00	50.80	114.62	.00	.00	29.84	
	13.68						

RCC	.00	50.80	114.62	.00	.00	29.84	
	10.68						
RCC	.00	50.80	114.62	.00	.00	29.84	
	3.68						
RCC	.00	50.80	144.78	.00	.00	30.48	SENSORS
	20.00						
RCC	.00	50.80	145.10	.00	.00	29.84	
	19.68						
RCC	.00	50.80	145.10	.00	.00	29.84	
	15.68						
RCC	.00	50.80	145.10	.00	.00	29.84	
	5.68						
RCC	.00	50.80	175.26	.00	.00	18.64	HEAD
	4.66						
TRC	-50.80	.00	22.86	.00	.00	30.48	NOZZLE
	20.00	14.0					
TRC	-50.80	.00	22.86	.00	.00	30.48	
	19.68	13.68					
RCC	-50.80	.00	53.34	.00	.00	15.24	MOTOR
	14.00						
RCC	-50.80	.00	53.66	.00	.00	14.92	
	13.68						
RCC	-50.80	.00	68.58	.00	.00	45.72	FUEL TANK
	20.00						
RCC	-50.80	.00	68.90	.00	.00	45.08	
	19.68						
RCC	-50.80	.00	114.30	.00	.00	30.48	COMPUTR
	14.00						
RCC	-50.80	.00	114.62	.00	.00	29.84	
	13.68						
RCC	-50.80	.00	114.62	.00	.00	29.84	
	10.68						
RCC	-50.80	.00	114.62	.00	.00	29.84	
	3.68						
RCC	-50.80	.00	144.78	.00	.00	30.48	SENSORS
	20.00						
RCC	-50.80	.00	145.10	.00	.00	29.84	
	19.68						
RCC	-50.80	.00	145.10	.00	.00	29.84	
	15.68						
RCC	-50.80	.00	145.10	.00	.00	29.84	
	5.68						
RCC	-50.80	.00	175.26	.00	.00	18.64	HEAD
	4.66						
TRC	.00	-50.80	22.86	.00	.00	30.48	NOZZLE
	20.00	14.0					
TRC	.00	-50.80	22.86	.00	.00	30.48	
	19.68	13.68					
RCC	.00	-50.80	53.34	.00	.00	15.24	MOTOR
	14.00						
RCC	.00	-50.80	53.66	.00	.00	14.92	
	13.68						
RCC	.00	-50.80	68.58	.00	.00	45.72	FUEL TANK
	20.00						

RCC	.00	-50.80	68.90	.00	.00	45.08	
	19.68						
RCC	.00	-50.80	114.30	.00	.00	30.48	COMPUTR
	14.00						
RCC	.00	-50.80	114.62	.00	.00	29.84	
	13.68						
RCC	.00	-50.80	114.62	.00	.00	29.84	
	10.68						
RCC	.00	-50.80	114.62	.00	.00	29.84	
	3.68						
RCC	.00	-50.80	144.78	.00	.00	30.48	SENSORS
	20.00						
RCC	.00	-50.80	145.10	.00	.00	29.84	
	19.68						
RCC	.00	-50.80	145.10	.00	.00	29.84	
	15.68						
RCC	.00	-50.80	145.10	.00	.00	29.84	
	5.68						
RCC	.00	-50.80	175.26	.00	.00	18.64	HEAD
	4.66						
TRC	.00	.00	22.86	.00	.00	30.48	NOZZLE
	20.00	14.0					
TRC	.00	.00	22.86	.00	.00	30.48	
	19.68	13.68					
RCC	.00	.00	53.34	.00	.00	15.24	MOTOR
	14.00						
RCC	.00	.00	53.66	.00	.00	14.92	
	13.68						
RCC	.00	.00	68.58	.00	.00	45.72	FUEL TANK
	20.00						
RCC	.00	.00	68.90	.00	.00	45.08	
	19.68						
RCC	.00	.00	114.30	.00	.00	30.48	COMPUTR
	14.00						
RCC	.00	.00	114.62	.00	.00	29.84	
	13.68						
RCC	.00	.00	114.62	.00	.00	29.84	
	10.68						
RCC	.00	.00	114.62	.00	.00	29.84	
	3.68						
RCC	.00	.00	144.78	.00	.00	30.48	SENSORS
	20.00						
RCC	.00	.00	145.10	.00	.00	29.84	
	19.68						
RCC	.00	.00	145.10	.00	.00	29.84	
	15.68						
RCC	.00	.00	145.10	.00	.00	29.84	
	5.68						
RCC	.00	.00	175.26	.00	.00	18.64	HEAD
	4.66						
TRC	50.80	.00	-22.86	.00	.00	-30.48	NOZZLE
	20.00	14.0					
TRC	50.80	.00	-22.86	.00	.00	-30.48	
	19.68	13.68					

RCC	50.80	.00	-53.34	.00	.00	-15.24	MOTOR
	14.00						
RCC	50.80	.00	-53.66	.00	.00	-14.92	
	13.68						
RCC	50.80	.00	-68.58	.00	.00	-45.72	FUEL TANK
	20.00						
RCC	50.80	.00	-68.90	.00	.00	-45.08	
	19.68						
RCC	50.80	.00	-114.30	.00	.00	-30.48	COMPUTR
	14.00						
RCC	50.80	.00	-114.62	.00	.00	-29.84	
	13.68						
RCC	50.80	.00	-114.62	.00	.00	-29.84	
	10.68						
RCC	50.80	.00	-114.62	.00	.00	-29.84	
	3.68						
RCC	50.80	.00	-144.78	.00	.00	-30.48	SENSORS
	20.00						
RCC	50.80	.00	-145.10	.00	.00	-29.84	
	19.68						
RCC	50.80	.00	-145.10	.00	.00	-29.84	
	15.68						
RCC	50.80	.00	-145.10	.00	.00	-29.84	
	5.68						
RCC	50.80	.00	-175.26	.00	.00	-18.64	HEAD
	4.66						
TRC	.00	50.80	-22.86	.00	.00	-30.48	NOZZLE
	20.00	14.0					
TRC	.00	50.80	-22.86	.00	.00	-30.48	
	19.68	13.68					
RCC	.00	50.80	-53.34	.00	.00	-15.24	MOTOR
	14.00						
RCC	.00	50.80	-53.66	.00	.00	-14.92	
	13.68						
RCC	.00	50.80	-68.58	.00	.00	-45.72	FUEL TANK
	20.00						
RCC	.00	50.80	-68.90	.00	.00	-45.08	
	19.68						
RCC	.00	50.80	-114.30	.00	.00	-30.48	COMPUTR
	14.00						
RCC	.00	50.80	-114.62	.00	.00	-29.84	
	13.68						
RCC	.00	50.80	-114.62	.00	.00	-29.84	
	10.68						
RCC	.00	50.80	-114.62	.00	.00	-29.84	
	3.68						
RCC	.00	50.80	-144.78	.00	.00	-30.48	SENSORS
	20.00						
RCC	.00	50.80	-145.10	.00	.00	-29.84	
	19.68						
RCC	.00	50.80	-145.10	.00	.00	-29.84	
	15.68						
RCC	.00	50.80	-145.10	.00	.00	-29.84	
	5.68						

RCC	.00	50.80	-175.26	.00	.00	-18.64	HEAD
	4.66						
TRC	-50.80	.00	-22.86	.00	.00	-30.48	NOZZLE
	20.00	14.0					
TRC	-50.80	.00	-22.86	.00	.00	-30.48	
	19.68	13.68					
RCC	-50.80	.00	-53.34	.00	.00	-15.24	MOTOR
	14.00						
RCC	-50.80	.00	-53.66	.00	.00	-14.92	
	13.68						
RCC	-50.80	.00	-68.58	.00	.00	-45.72	FUEL TANK
	20.00						
RCC	-50.80	.00	-68.90	.00	.00	-45.08	
	19.68						
RCC	-50.80	.00	-114.30	.00	.00	-30.48	COMPUTR
	14.00						
RCC	-50.80	.00	-114.62	.00	.00	-29.84	
	13.68						
RCC	-50.80	.00	-114.62	.00	.00	-29.84	
	10.68						
RCC	-50.80	.00	-114.62	.00	.00	-29.84	
	3.68						
RCC	-50.80	.00	-144.78	.00	.00	-30.48	SENSORS
	20.00						
RCC	-50.80	.00	-145.10	.00	.00	-29.84	
	19.68						
RCC	-50.80	.00	-145.10	.00	.00	-29.84	
	15.68						
RCC	-50.80	.00	-145.10	.00	.00	-29.84	
	5.68						
RCC	-50.80	.00	-175.26	.00	.00	-18.64	HEAD
	4.66						
TRC	.00	-50.80	-22.86	.00	.00	-30.48	NOZZLE
	20.00	14.0					
TRC	.00	-50.80	-22.86	.00	.00	-30.48	
	19.68	13.68					
RCC	.00	-50.80	-53.34	.00	.00	-15.24	MOTOR
	14.00						
RCC	.00	-50.80	-53.66	.00	.00	-14.92	
	13.68						
RCC	.00	-50.80	-68.58	.00	.00	-45.72	FUEL TANK
	20.00						
RCC	.00	-50.80	-68.90	.00	.00	-45.08	
	19.68						
RCC	.00	-50.80	-114.30	.00	.00	-30.48	COMPUTR
	14.00						
RCC	.00	-50.80	-114.62	.00	.00	-29.84	
	13.68						
RCC	.00	-50.80	-114.62	.00	.00	-29.84	
	10.68						
RCC	.00	-50.80	-114.62	.00	.00	-29.84	
	3.68						
RCC	.00	-50.80	-144.78	.00	.00	-30.48	SENSORS
	20.00						

RCC	.00	-50.80	-145.10	.00	.00	-29.84	
	19.68						
RCC	.00	-50.80	-145.10	.00	.00	-29.84	
	15.68						
RCC	.00	-50.80	-145.10	.00	.00	-29.84	
	5.68						
RCC	.00	-50.80	-175.26	.00	.00	-18.64	HEAD
	4.66						
TRC	.00	.00	-22.86	.00	.00	-30.48	NOZZLE
	20.00	14.0					
TRC	.00	.00	-22.86	.00	.00	-30.48	
	19.68	13.68					
RCC	.00	.00	-53.34	.00	.00	-15.24	MOTOR
	14.00						
RCC	.00	.00	-53.66	.00	.00	-14.92	
	13.68						
RCC	.00	.00	-68.58	.00	.00	-45.72	FUEL TANK
	20.00						
RCC	.00	.00	-68.90	.00	.00	-45.08	
	19.68						
RCC	.00	.00	-114.30	.00	.00	-30.48	COMPUTR
	14.00						
RCC	.00	.00	-114.62	.00	.00	-29.84	
	13.68						
RCC	.00	.00	-114.62	.00	.00	-29.84	
	10.68						
RCC	.00	.00	-114.62	.00	.00	-29.84	
	3.68						
RCC	.00	.00	-144.78	.00	.00	-30.48	SENSORS
	20.00						
RCC	.00	.00	-145.10	.00	.00	-29.84	
	19.68						
RCC	.00	.00	-145.10	.00	.00	-29.84	
	15.68						
RCC	.00	.00	-145.10	.00	.00	-29.84	
	5.68						
RCC	.00	.00	-175.26	.00	.00	-18.64	HEAD
	4.66						
BOX	1.25	81.60	-15.24	-2.50	0.0	0.0	PANEL CN
	0.0	20.00	0.0	0.0	0.0	30.48	
BOX	2.50	101.60	-170.69	-5.00	0.0	0.0	RT SLR P
	0.0	170.69	0.0	0.0	0.0	341.38	
BOX	1.25	-81.60	-15.24	-2.50	0.0	0.0	PANEL CN
	0.0	-20.00	0.0	0.0	0.0	30.48	
BOX	2.50	-101.60	-170.69	-5.00	0.0	0.0	LT SLR P
	0.0	-170.69	0.0	0.0	0.0	341.38	
RCC	0.0	0.0	-15.24	0.0	0.0	-198.12	
	81.60						
RCC	0.0	0.0	-15.24	0.0	0.0	-197.80	
	81.28						
BOX	82.60	-50.800	-213.360	-1.000	0.00	0.00	
	0.0	101.600	0.0	0.0	0.0	426.720	
BOX	82.60	-50.800	-213.360	-0.441	0.897	0.0	
	-71.781	-35.320	0.0	0.0	0.0	426.720	

```
BOX           82.60     50.800  -213.360    -0.441    -0.897     0.0
             -71.781    35.320     0.0       0.0       0.0     426.720
RCC          -81.600     0.0       0.0     -50.0       0.0     000.000
               5.000
RCC         -131.600     0.0       0.0     -10.0       0.0       0.0
              35.000
END
EXT   600      +1      -2
SPH            +2      -3      -5     -73     -74     -75     -76     -77     -78
              -79     -80     -81     -82    -233    -234    -235    -236    -237
             -239    -240    -241    -242    -243
PLT            +3      -4      -5    -233    -235     -57     -58     -59     -60
              -61     -62     -63     -64    -239    -240    -241
PTL            +4      -5     -21     -23     -25     -27     -29     -31     -33
              -35     -37     -39     -41     -43     -45     -47     -49     -51
              -53     -55     -57     -58     -59     -60     -61     -62     -63
              -64     -65     -66     -67     -68     -69     -70     -71     -72
IBY            +5      -6     -21     -23     -25     -27     -29     -31     -33
              -35     -37     -39     -41     -43     -45     -47     -49     -51
              -53     -17     -18     -19     -20    -239    -240    -241    -242
IBV            +6      -7      -8      -9     -10     -11     -12     -13     -14
              -15     -16     -17     -18     -19     -20
IBL            +7      -8     -17     -18     -19     -20
INS            +8      -9
IBL            +9     -10
INS           +10     -11
IBL           +11     -12
INS           +12     -13
IBL           +13     -14
IBV           +14     -15
BOX           +15     -16
BXV           +16
ISB           +17
ISB           +18
ISB           +19
ISB           +20
FT1           +21      -5     -22
FIT           +22      -5     -83     -84     -85     -87     -89     -93     -97
FT2           +23      -5     -24
FIT           +24      -5
FT3           +25      -5     -26
FIT           +26      -5     -98     -99    -100    -102    -104    -108    -112
FT4           +27      -5     -28
FIT           +28      -5
FT5           +29      -5     -30
FIT           +30      -5    -113    -114    -115    -117    -119    -123    -127
FT6           +31      -5     -32
FIT           +32      -5
FT7           +33      -5     -34
FIT           +34      -5    -128    -129    -130    -132    -134    -138    -142
FT8           +35      -5     -36
FIT           +36      -6
FT9           +37      -5     -38
FIT           +38      -5    -143    -144    -145    -147    -149    -153    -157
```

BT1	+39	-5	-40						
BIT	+40	-5	-158	-159	-160	-162	-164	-168	-172
BT2	+41	-5	-42						
BIT	+42	-5							
BT3	+43	-5	-44						
BIT	+44	-5	-173	-174	-175	-177	-179	-183	-187
BT4	+45	-5	-46						
BIT	+46	-5							
BT5	+47	-5	-48						
BIT	+48	-5	-188	-189	-190	-192	-194	-198	-202
BT6	+49	-5	-50						
BIT	+50	-5							
BT7	+51	-5	-52						
BIT	+52	-5	-203	-204	-205	-207	-209	-213	-217
BT8	+53	-5	-54						
BIT	+54	-5							
BT9	+55	-5	-56						
BIT	+56	-5	-218	-219	-220	-222	-224	-228	-232
FB1	+57	-5	-37	-21					
FB2	+58	-5	-37	-23					
FB3	+59	-5	-37	-25					
FB4	+60	-5	-37	-27					
FB5	+61	-5	-37	-29					
FB6	+62	-5	-37	-31					
FB7	+63	-5	-37	-33					
FB8	+64	-5	-37	-35					
BB1	+65	-5	-55	-39					
BB2	+66	-5	-55	-41					
BB3	+67	-5	-55	-43					
BB4	+68	-5	-55	-45					
BB5	+69	-5	-55	-47					
BB6	+70	-5	-55	-49					
BB7	+71	-5	-55	-51					
BB8	+72	-5	-55	-53					
FC1	+73	-3	-21	-22					
FC3	+74	-3	-25	-26					
FC5	+75	-3	-29	-30					
FC7	+76	-3	-33	-34					
FC9	+77	-3	-37	-38					
BC1	+78	-3	-39	-40					
BC3	+79	-3	-43	-44					
BC5	+80	-3	-47	-48					
BC7	+81	-3	-51	-52					
BC9	+82	-3	-55	-56					
KV1	83	-84							
KV1	84								
KV1	85	-83	-86						
KV1	86								
KV1	87	-85	-88	-86					
KV1	88								
KV1	89	-87	-90						
KV1	90	-91	-92						
KV1	91	-92							
KV1	92	-93							

KV1	93	-94	-89	
KV1	94	-95	-96	
KV1	95	-96		
KV1	96			
KV1	97	-93		
KV2	98	-99		
KV2	99			
KV2	100	-98	-101	
KV2	101			
KV2	102	-100	-103	-101
KV2	103			
KV2	104	-102	-105	
KV2	105	-106	-107	
KV2	106	-107		
KV2	107	-108		
KV2	108	-109	-104	
KV2	109	-110	-111	
KV2	110	-111		
KV2	111			
KV2	112	-108		
KV3	113	-114		
KV3	114			
KV3	115	-113	-116	
KV3	116			
KV3	117	-115	-118	-116
KV3	118			
KV3	119	-117	-120	
KV3	120	-121	-122	
KV3	121	-122		
KV3	122	-123		
KV3	123	-124	-119	
KV3	124	-125	-126	
KV3	125	-126		
KV3	126			
KV3	127	-123		
KV4	128	-129		
KV4	129			
KV4	130	-128	-131	
KV4	131			
KV4	132	-130	-133	-131
KV4	133			
KV4	134	-132	-135	
KV4	135	-136	-137	
KV4	136	-137		
KV4	137	-138		
KV4	138	-139	-134	
KV4	139	-140	-141	
KV4	140	-141		
KV4	141			
KV4	142	-138		
KV5	143	-144		
KV5	144			
KV5	145	-143	-146	
KV5	146			

KV5	147	-145	-148	-146
KV5	148			
KV5	149	-147	-150	
KV5	150	-151	-152	
KV5	151	-152		
KV5	152	-153		
KV5	153	-154	-149	
KV5	154	-155	-156	
KV5	155	-156		
KV5	156			
KV5	157	-153		
KV6	158	-159		
KV6	159			
KV6	160	-158	-161	
KV6	161			
KV6	162	-160	-163	-161
KV6	163			
KV6	164	-162	-165	
KV6	165	-166	-167	
KV6	166	-167		
KV6	167	-168		
KV6	168	-169	-164	
KV6	169	-170	-171	
KV6	170	-171		
KV6	171			
KV6	172	-168		
KV7	173	-174		
KV7	174			
KV7	175	-173	-176	
KV7	176			
KV7	177	-175	-178	-176
KV7	178			
KV7	179	-177	-180	
KV7	180	-181	-182	
KV7	181	-182		
KV7	182	-183		
KV7	183	-184	-179	
KV7	184	-185	-186	
KV7	185	-186		
KV7	186			
KV7	187	-183		
KV8	188	-189		
KV8	189			
KV8	190	-188	-191	
KV8	191			
KV8	192	-190	-193	-191
KV8	193			
KV8	194	-192	-195	
KV8	195	-196	-197	
KV8	196	-197		
KV8	197	-198		
KV8	198	-199	-194	
KV8	199	-200	-201	
KV8	200	-201		

```
KV8      201
KV8      202   -198
KV9      203   -204
KV9      204
KV9      205   -203   -206
KV9      206
KV9      207   -205   -208   -206
KV9      208
KV9      209   -207   -210
KV9      210   -211   -212
KV9      211   -212
KV9      212   -213
KV9      213   -214   -209
KV9      214   -215   -216
KV9      215   -216
KV9      216
KV9      217   -213
KVA      218   -219
KVA      219
KVA      220   -218   -221
KVA      221
KVA      222   -220   -223   -221
KVA      223
KVA      224   -222   -225
KVA      225   -226   -227
KVA      226   -227
KVA      227   -228
KVA      228   -229   -224
KVA      229   -230   -231
KVA      230   -231
KVA      231
KVA      232   -228
SPC      233   -234
SP1      234
SPC      235   -236
SP2      236
BPL     +237   -238    -39    -40    -41    -43    -44    -45    -47
         -48    -49    -51    -52    -55    -56    -78    -79    -53
         -80    -81    -82     -5   -239   -240   -241
PLB     +238     -5    -39    -41    -43    -45    -47    -49    -51
         -53    -55    -65    -66    -67    -68    -69    -70    -71
         -72    -78    -79    -80    -81    -82
BLP      239
LLP      240   -239
RLP      241   -239
ASB      242
ANT      243   -242
END
   1   1   1   1   1   1   1   1   1   1   1   1   1   1
   1   1   1   1   1   1   1   1   1   1   1   1   1   1
   1   1   1   1   1   1   1   1   1   1   1   1   1   1
   1   1   1   1   1   1   1   1   1   1   1   1   1   1
   1   1   1   1   1   1   1   1   1   1   1   1   1   1
   1   1   1   1   1   1   1   1   1   1   1   1   1   1
```

1	1	1	1	1	1	1	1	1	1	1	1	1	1
1	1	1	1	1	1	1	1	1	1	1	1	1	1
1	1	1	1	1	1	1	1	1	1	1	1	1	1
1	1	1	1	1	1	1	1	1	1	1	1	1	1
1	1	1	1	1	1	1	1	1	1	1	1	1	1
1	1	1	1	1	1	1	1	1	1	1	1	1	1
1	1	1	1	1	1	1	1	1	1	1	1	1	1
1	1	1	1	1	1	1	1	1	1	1	1	1	1
1	1	1	1	1	1	1	1	1	1	1	1	1	1
1	1	1	1	1	1	1	1	1	1	1	1	1	1
1	1	1	1	1	1	1	1	1	1	1	1	1	1
1	1	1	1	1									
0	9	1	9	1	9	1	2	1	9	1	2	1	9
1	2	1	1	1	1	1	9	1	4	1	9	1	4
1	9	1	4	1	9	1	4	1	9	1	9	1	4
1	9	1	4	1	9	1	4	1	9	1	4	1	9
1	1	1	1	1	1	1	1	1	1	1	1	1	1
1	1	1	1	1	1	1	1	1	1	1	1	1	9
1	7	1	3	1	9	2	9	1	9	2	9	8	1
9	1	7	1	3	1	9	2	9	1	9	2	9	8
1	9	1	7	1	3	1	9	2	9	1	9	2	9
8	1	9	1	7	1	3	1	9	2	9	1	9	2
9	8	1	9	1	7	1	3	1	9	2	9	1	9
2	9	8	1	9	1	7	1	3	1	9	2	9	1
9	2	9	8	1	9	1	7	1	3	1	9	2	9
1	9	2	9	8	1	9	1	7	1	3	1	9	2
9	1	9	2	9	8	1	9	1	7	1	3	1	9
2	9	1	9	2	9	8	1	9	1	7	1	3	1
9	2	9	1	9	2	9	8	1	5	1	5	1	9
6	6	6	1	2									

REFERENCES

1. T. A. Gabriel, "The High Energy Transport Code HETC," ORNL/TM-9727, Oak Ridge National Laboratory, (September 1985).
2. M. B. Emmett, "MORSE-CGA, A Monte Carlo Radiation Transport Code with Array Geometry Capability," ORNL-6174, Oak Ridge National Laboratory, (April 1985).
3. J. O. Johnson and T. A. Gabriel, "Development and Evaluation of a Monte Carlo Code System for Analysis of Ionization Chamber Responses," ORNL/TM-10196, Oak Ridge National Laboratory, (July 1987).
4. Walter R. Nelson, Hideo Hirayama, and David W. O. Rogers, "The EGS4 Code System," SLAC-265 (December 1985).
5. M. B. Emmett, L. M. Petrie, and J. T. West, "JUNEBUG-II — A Three Dimensional Geometry Plotting Code," NUREG/CR-0200, Vol. 2, Section F12, ORNL/NUREG-CSD-2/V2/R (December 1984).
6. C. E. McIlwain, "Coordinates for Mapping of Magnetically Trapped Particles," *J. Geophys. Research* **66**, 3681 (1968).
7. "Data User's Note: TRECO, An Orbital Integration Computer Code for Trapped Radiation," National Space Science Data Center, Goddard Space Flight Center, NASA Document NSSDC-68-02) (1968).
8. CPT Roman B. Zacharko, "High Altitude Nuclear Burst Electron Fluence and Dose Calculations for a Parametric Set of Orbits," External Correspondance, Air Force Weapons Laboratory, Kirtland Air Force Base, New Mexico.
9. T. A. Gabriel, et al., "The Oak Ridge National Laboratory Strategic Defense Initiative Shield Optimization Program," Oak Ridge National Laboratory, ORNL/TM-10631, April 1988.
10. J. O. Johnson, T. A. Gabriel, J. M. Barnes, J. D. Drischler, M. S. Smith, and R. T. Santoro, "Shield Optimization Program, Part III: Effects of X-Ray Radiation From Nuclear Weapons on SDI Weapon Platforms," Oak Ridge National Laboratory, ORNL/TM-10962.
11. M. S. Smith, J. O. Johnson, T. A. Gabriel, J. M. Barnes, J. D. Drischler, and R. T. Santoro, "Shield Optimization Program, Part IV: Effects of Neutron and Gamma-Ray Radiations from Nuclear Weapons on SDI Weapon Platforms," Oak Ridge National Laboratory, ORNL/TM-10963.
12. M. S. Smith, T. J. Burns, J. O. Johnson, J. M. Barnes, J. D. Drischler, T. A. Gabriel, and R. T. Santoro, "Shield Optimization Program, Part V: A Hydrodynamic Comparison Using HULL and PUFF-TFT for a One-Dimensional Aluminum Slab," Oak Ridge National Laboratory, ORNL/TM-10964.